Water Science & Technology

Water Science & Technology Vol 87 No 9, 2277 doi: 10.2166/wst.2023.101

Remediation of Pb (II), Cd (II), and Zn (II) from aqueous solutions using porous (styrene–divinylbenzene)/Cu–Ni bimetallic nanocomposite microspheres: continuous fixed-bed column study

Hridya Thrikkykkal, Rosmin Antu and Harikumar P. S.*

Ecology and Environment Research Group, Centre for Water Resources Development and Management, Kunnamangalam, Kozhikode, Kerala 673 571, India
*Corresponding author. E-mail: drpshari@yahoo.co.in

ABSTRACT

Bimetallic nanoparticles (BNPs) have been used as a new line of defence against heavy metal contamination among several types of nanoparticles (NPs) due to their enhanced, synergistic activity. In this study, we investigated the adsorption behaviour of porous (styrene–divinylbenzene)/CuNi bimetallic nanocomposite (P(St-DVB)/CuNi BNC) in a continuous flow fixed-bed column and its ability to remove Pb (II), Cd (II), and Zn (II) ions from aqueous solutions. We examined how the initial metal concentration, flow rate, and bed height affected the adsorption characteristics. Experimental results confirmed that the adsorption capacity increased with increase in influent metal concentration and bed height and decreased with increase in flow rate. The breakthrough and the column kinetic parameters were successfully predicted with three mathematical models: Thomas, Yoon–Nelson, and Adams–Bohart models. Both Thomas and Yoon–Nelson models showed good agreement with the experimental results for all the operating conditions. Successful desorption of heavy metals from the P(St-DVB)/CuNi BNC was performed using 0.5 M NaOH solution, and it showed good reusability of the adsorbent during four adsorption–desorption cycles. The results show that P(St-DVB)/CuNi BNC are effective and low-cost adsorbents, and they can be used in real-time large-scale industrial water treatment processes for the removal of heavy metals.

Key words: adsorption, bimetallic nanoparticle, breakthrough curve, fixed-bed column, heavy metal removal, styrene–divinylbenzene nanocomposite

HIGHLIGHTS

- Fixed-bed column was used for the removal of Pb (II), Cd (II), and Zn (II) using poly(styrene–divinylbenzene)/CuNi nanocomposite (P(St-DVB)/CuNi BNC) microspheres, which was found to be efficient and low-cost adsorbent.
- 87, 85, and 92% removal efficiencies were achieved for lead, cadmium, and zinc, respectively.
- Conducted successful desorption of heavy metals from the P(St-DVB)/CuNi BNC.

GRAPHICAL ABSTRACT

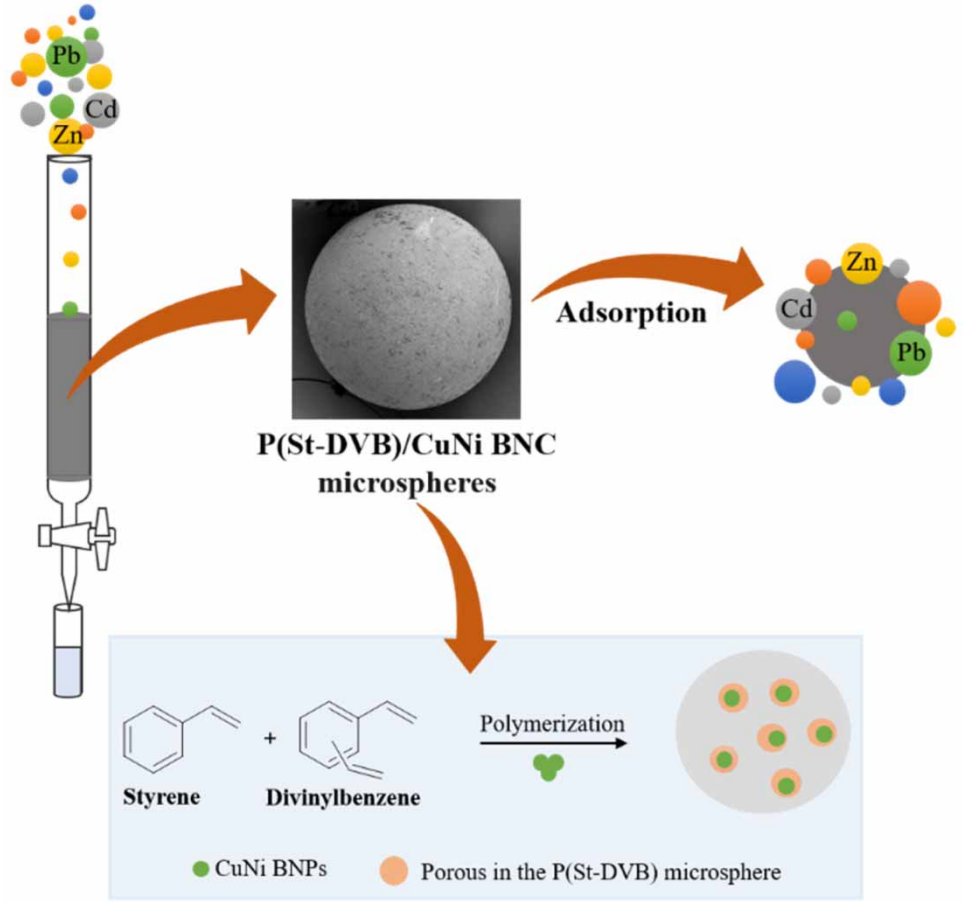

1. INTRODUCTION

Clean and fresh water is the most essential element for the survival of all forms of life on Earth. It is considered the most precious resource in this world, and its scarcity, in terms of quantity and quality, has become a significant threat to the well-being of people (Rijsberman 2006). The progressive explosion of global population growth increases the demand for clean and potable water (Sandia 2003; Chen *et al.* 2016). Moreover, the ever-expanding increase in industrialisation, rapid urbanisation, and increase in water contamination add enormously to the existing problems of water scarcity by contaminating large volumes of available water, and it does not seem easy to make further improvements (McNabb 2019; Omer *et al.* 2020). Hence, the management and control of contaminants have become a major environmental concern for national and international organisations, governments, and researchers throughout the world (Olvera *et al.* 2017).

In contrast to organic contaminants, heavy metals are toxic, carcinogenetic, and non-biodegradable. In addition, they can accumulate in living tissues due to their non-biodegradable character and become concentrated in internal organs such as the brain, kidneys, and liver (Pehlivan *et al.* 2008; Schwarzenbach *et al.* 2010). These concentrated metals can affect the functioning of vital body organs and cause a range of health problems including neurological damage, cancer, kidney failure, etc. Moreover, heavy metals are considered conservative pollutants that are not subjected to bacterial attack or other breakdown or degradation processes and hence are a permanent addition to the environment. Untreated or partially treated wastewater discharge from industries such as metal plating industries, mining, leather tanning, textile dyeing, paints, pigment manufacturing, batteries, fertilisers, water cooling and electroplating is the prime root of heavy metal contamination by human contribution (Tchounwou *et al.* 2012). These heavy metals, released from such contaminated areas, can easily be transported through the environment and leached into the nearby surface

and groundwater. This can usually result in the spread of these metals over vast areas and form large-scale contamination (Nriagu & Pacyna 1988). Therefore, effective treatment of heavy metal-contaminated wastewater is a prerequisite before it is discharged into the environment.

Many of the commonly used drinking water treatment techniques, including chlorination, boiling, and solar disinfection, are ineffective at removing these heavy metals (De Kwaadsteniet *et al.* 2013). Therefore, the treatment of heavy metals is of special concern for the substantial growth of humans and the environment. In recent years, several wastewater treatment techniques have been developed to mitigate the problem of heavy metal contamination from aqueous medium. However, these methods still have some limitations, especially high operation cost, incomplete removal, and low efficiency (Barakat 2011). Cheaper and more efficient approaches have been studied to advance the quality of effluents.

Currently, BNPs have been used as a new line of defence against heavy metal contamination among various types of NPs due to their enhanced and synergistic activity and better efficiency compared to the constituent ingredients (Taner *et al.* 2011). Furthermore, a low concentration of bimetallic nanoparticles has been reported to exhibit better adsorption properties than a single metallic nanoparticle (Sharma *et al.* 2015; Sharma *et al.* 2019; Wadhawan *et al.* 2020). Our previous study has shown that CuNi BNPs have a higher adsorption efficiency for heavy metals than individual Cu and Ni NPs, as well as most of the other nanoadsorbents (Harikumar & Hridya 2021). Furthermore, by immobilising CuNi BNPs in porous (styrene–divinylbenzene) copolymer, we were able to decrease and control the release rate of NPs, as well as provide efficient protection against NP oxidation and agglomeration, which in turn increased its adsorption capacity. All these investigations on heavy metal removal focused only on batch equilibrium and kinetic studies (Harikumar & Hridya 2021; Hridya *et al.* 2021). However, batch studies provide useful information; such data are limited to laboratory processes and may not apply to most of the long-term treatment systems (Agrawal & Bajpai 2011; Li *et al.* 2011). However, continuous column studies provide the most practical data for real-field applications, and they can be easily scaled up from a laboratory scale to an industrial scale (Aksu & Gönen 2004).

Consequently, as a continuation of our previous research, the present study was carried out to evaluate the potential of a porous (styrene–divinylbenzene)/CuNi bimetallic nanocomposite (P(St-DVB)/CuNi BNC) in a fixed-bed adsorption column to remove heavy metals such as Pb, Cd, and Zn from contaminated water. The objectives of this study are (1) to investigate the effects of flow rate, influent metal concentration, and bed height on the adsorption capacity and the heavy metal removal efficiency by P(St-DVB)/CuNi BNC, (2) to analyse the obtained breakthrough curves obtained using existing model equations such as Thomas, Yoon–Nelson, and Adams–Bohart models, and (3) to evaluate the reusability of the packed column by performing a series of successive adsorption–desorption cycles.

2. MATERIALS AND METHODS

2.1. Materials

All of the chemicals used in the study were obtained from Merck in India and were of analytical reagent grade. Thermofisher inductively coupled plasma optical emission spectroscopy (ICP-OES, iCAP7400 Duo MFC) was used to analyse the heavy metals. Contaminated aqueous solutions of heavy metals were prepared by diluting the corresponding metal standard stock solutions. 0.1 M HCl and 0.1 M NaOH were used for pH adjustments.

2.2. Preparation of the poly(styrene–divinylbenzene)/CuNi nanocomposite

The detailed procedure for the synthetisation of CuNi BNP was given in our previous report (Harikumar & Hridya 2021). P(St-DVB)/CuNi BNC microbeads were prepared via the *in situ* oil-in-water emulsion polymerisation technique. To prepare P(St-DVB)/CuNi BNC, 3 g of previously prepared CuNi BNPs were added to 50 mL of deionised water in a beaker and ultrasonicated for 10 min for better dispersion of bimetallic nanoparticles in water. 300 mL of an aqueous solution of 0.5% polyvinyl alcohol along with the deionised water containing CuNi BNP was added to a 500 mL round bottom flask equipped with a magnetic stir bar and reflux condenser. The temperature was raised to around 65 °C and a monomer mixture containing styrene (75 mL), divinylbenzene (3 mL), and benzoyl peroxide (3 g) as the initiator was added dropwise using a micropipette to this solution for polymerisation and bead creation. The temperature was then raised to 90 °C and kept constant until polymerisation was completed (6 h). After the reaction period, the bead was filtered, washed several times with deionised water (total 2 L) and methanol (total 400 mL), and finally dried.

2.3. Characterisation of adsorbent

The surface morphology features of the adsorbent were identified by field emission scanning electron microscopy (FE-SEM) supported by energy-dispersive X-ray spectroscopy (FE-SEM-EDX, ZEISS GeminiSEM 300) and high-resolution transmission electron microscope (HR-TEM, Jeol/JEM 2100). For structural characterisation, XRD patterns were measured (PXRD, Bruker D8 Advance). The surface area was measured using the Brunauer–Emmett–Teller method (BET, BELSORP-max) using nitrogen as the adsorbate.

2.4. Continuous adsorption studies

Continuous adsorption studies were conducted to evaluate the performance of a fixed-bed adsorption column. A glass column with an internal diameter of 2 cm and a length of 30 cm was used for laboratory-scale column experiments. The column was designed on the data from our earlier batch-scale experiments. The desired quantity of P(St-DVB)/CuNi BNC microspheres was packed as an interlayer between two supporting layers of glass wool to prevent any loss of adsorbent during elution. After filling, the columns were initially flushed with distilled water in a down flow mode for 1 h, to rinse and equilibrate the adsorbent particles. Experiments were carried out by pumping the heavy metal solution of known concentrations through the column at room temperature (298 K) and an optimal pH. The effluent was collected from the column's outflow regularly and kept for analysis. The concentration of heavy metals present in the column effluent samples was measured using ICP-OES. To ensure the accuracy and reproducibility of all the data, each experiment was performed in triplicate and the mean values were used in the data analysis. The percentage standard deviation of the experiments was calculated. The effect of various process parameters, such as initial concentration, flow rate, and bed height, on the breakthrough curves and amount of metal removed were investigated. The experimental conditions in Table 1 were varied to quantitatively evaluate their effects on metal adsorption.

The performance of the adsorption column is conveniently described through the concept of the breakthrough curve (Aksu *et al.* 2007). A plot of the ratio of concentrations (C_t/C_0) versus time (t) or volume (v) of the effluent is known as the breakthrough curve (C_t/C_0 versus time). The breakthrough curves illustrate the performance of fixed-bed columns, and the time to reach the breakthrough and shape of the breakthrough curve are the key characteristics for evaluating the adsorption capacity of a column because they directly affect the feasibility and economics of the adsorption process (Ahmad & Hameed 2010). An ideal breakthrough curve has a symmetric sigmoidal shape (S-shape) and the time required for the effluent concentration to reach 10% of the input concentration ($C_t/C_0 = 0.1$) was defined as the breakthrough point time (t_b). Table 2 represents various breakthrough parameters and their equations for determination (Luo *et al.* 2011; Nuić *et al.* 2013; Yagub *et al.* 2015).

2.5. Mathematical modelling of breakthrough curves

The prediction of the breakthrough curve is important for scaling up the adsorption column. Several mathematical models have been proposed to investigate the mechanism of adsorption and the successful design of fixed-bed adsorption columns for industrial applications. The breakthrough curves obtained for initial metal ion concentration, flow rate, and bed height were studied using three well-known empirical models such as Thomas, Yoon–Nelson, and Bohart–Adams models.

Table 1 | Experimental condition for fixed-bed column study

Metals	Initial metal concentration (mg/L)	Flow rate (mL/min)	Bed height (cm)	pH
Pb	10, 50,100	2	2	5
	50	1,2,3	2	5
	50	2	2,4,6	5
Cd	10, 50,100	2	2	7
	50	1,2,3	2	7
	50	2	2,4,6	7
Zn	10, 50,100	2	2	7
	50	1,2,3	2	7
	50	2	2,4,6	7

Table 2 | Breakthrough parameters and their equations for determination

Breakthrough parameters	Equations	
Breakthrough time, t_b (min)	Time at $\frac{C_t}{C_0} = 0.1$	
Exhaust time, t_e (min)	Time at $\frac{C_t}{C_0} = 0.9$	
Column capacity, q_c (mg)	$q_c = \frac{QA}{1000} = \frac{Q}{1000}\int_0^t C_{ad}.dt$	Q and A are the flow rate (mL/min) and the area under the breakthrough curve, respectively. $C_{ad} = C_0 - C_e$, C_e is effluent metal ions concentration and C_0 is influent metal ions concentration (mg/L).
Total amount of metal ions sent to the column, m (mg)	$m = QC_0t_e$	
Percentage removal of metals	$\%R = \frac{q_c}{m} \times 100$	
Adsorption capacity, q (mg/g)	$q = \frac{q_c}{X}$	X is the total mass of the adsorbent in the column (g)
Length of mass transfer zone (MTZ) (cm)	$\mathrm{MTZ} = H\left(1 - \frac{t_b}{t_e}\right)$	H is total depth of the adsorbent in the column (cm).

2.5.1. Thomas model

The Thomas model is one of the most general and extensively used models for describing the column performance and predicting the breakthrough curve of metal adsorption in a fixed-bed column (Thomas 1944). The Thomas model follows the Langmuir adsorption–desorption model, i.e., no axial dispersion and is described by pseudosecond-order reversible reaction kinetics. This model is used to predict the adsorption rate constant and maximum uptake of the adsorbate. The Thomas model is mathematically expressed as follows:

$$\frac{C_t}{C_0} = \frac{1}{1 + \exp\left(\frac{k_{\mathrm{Th}}q_0m}{Q} - k_{\mathrm{Th}}C_0t\right)} \tag{1}$$

where C_0 is the concentration of influent adsorbate concentration (mg/L); C_t is the concentration of effluent at time t (mg/L); k_{Th} is the Thomas rate constant (mL/min mg); q_0 is the adsorption capacity (mg/g); m is the mass of the adsorbent (g), and Q is the flow rate (mL/min). The linearised form can be expressed in Equation (2):

$$\ln\left(\frac{C_0}{C_t} - 1\right) = \frac{k_{\mathrm{Th}}q_0m}{Q} - k_{\mathrm{Th}}C_0t \tag{2}$$

The slope and intercept of $\ln[(C_0/C_t)–1]$ versus the time t plot were used to calculate the values of k_{Th} and q_0.

2.5.2. Yoon–Nelson model

Yoon and Nelson established a reasonably simple model based on the premise that the rate of decline in the probability of adsorption for each adsorbate molecule was proportional to the probability of adsorption and the probability of adsorbate breakthrough on the adsorbent (Yoon & Nelson 1984). This model can be applied to evaluate the exhaustion time and the behaviour of the adsorption process for a given adsorbate concentration. The Yoon–Nelson model is mathematically expressed as follows:

$$\frac{C_t}{C_0} - C_t = \exp\left(k_{\mathrm{YN}}t - k_{\mathrm{YN}}\tau\right) \tag{3}$$

where k_{YN} is the Yoon–Nelson rate constant (min^{-1}), and the amount of time necessary to break down 50% of the adsorbate is defined as τ(min). The linearised form of the model is expressed in Equation (4):

$$\ln\left(\frac{C_t}{C_0 - C_t}\right) = k_{YN}t - \tau k_{YN} \tag{4}$$

The values of k_{YN} and τ can be determined from the slope and intercept of the linear graph of $\ln[C_t/(C_0–C_t)]$ against t.

2.5.3. Adams–Bohart model

The Adams–Bohart model was proposed by Bohart & Adams (1920) based on the surface reaction theory, and they developed an equation which successfully describes the relationship between C_t/C_0 and t in a continuous flow system of adsorption (Bohart & Adams 1920). It is based on the assumption that the rate of adsorption is proportional to the metal concentration, and the equilibrium is not instantaneous. This model describes the initial part of the breakthrough curve and the connection between C_t/C_0 and t in continuous systems. The model equation is expressed as

$$\frac{C_t}{C_0} = \exp\left(k_{AB}C_0t - k_{AB}N_0\frac{Z}{U_0}\right) \tag{5}$$

where k_{AB} is the Adams–Bohart rate constant (L mg^{-1} min^{-1}); N_0 is the saturation concentration (mg/L); z is the height of the bed (cm), and U_0 is the linear velocity (cm/min). The linearised form of the model is expressed in Equation (6):

$$\ln\left(\frac{C_t}{C_0}\right) = k_{AB}C_0t - k_{AB}N_0\left(\frac{Z}{U_0}\right) \tag{6}$$

2.6. Desorption experiments

To regenerate the adsorbent for further use, the columns were flushed with 0.5 M NaOH using a flow rate of 3.0 mL/min. After elution, the adsorbent bed was rinsed with deionised water for another 1 h with the same flow rate, and the regenerated bed was reused in another cycle. Desorption studies were conducted for up to four successive adsorption–desorption cycles.

3. RESULTS AND DISCUSSION

3.1. Characterisation of adsorbent

The detailed physicochemical characteristics of the P(St-DVB)/CuNi BNC microspheres have already been given in our previous report (Hridya *et al.* 2021). To examine the surface morphology of the microspheres, FE-SEM and high-resolution transmission electron microscopy (HR-TEM) micrographs were taken. The SEM image of the nanocomposite indicates the formation of spherical-shaped particles with an average diameter of 110 μm (Supplementary Figure S1(a) and (b)). It is interesting to note that P(St-DVB)/CuNi BNC particles with a larger size than those of CuNi bimetallic NPs were formed via encapsulation of CuNi bimetallic NPs by styrene and a divinylbenzene copolymer. The HR-TEM image was taken and is shown in Supplementary Figure S1(c). It is indicated that CuNi bimetallic NPs were successfully encapsulated within the P(St-DVB) microspheres. The darker core was CuNi bimetallic NPs, and their distribution in the microsphere was nonuniform. The entrapped NPs were almost spherical in shape and separated from each other. EDX was used to analyse the elemental constituents of the P(St-DVB)/CuNi BNC microspheres, and the results showed that Cu and Ni elements were present within the P(St-DVB) microsphere, and the weight percentages of C, Cu, and Ni were determined to be 78.98, 11.31, and 9.71, respectively (Supplementary Figure S2). The crystalline structure of the nanocomposite was characterised by PXRD as shown in Supplementary Figure S3. The P(St-DVB)/CuNi BNC microspheres showed prominent peaks at 43.26 (111), 50.44° (200), and 74.03° (220), confirming the crystal planes of CuNi BNPs (JCPDS # 3-065-7246). According to the BET analysis, the nanocomposite had a specific surface area of 25.88 m^2/g with an average pore diameter of 64.80 nm (Supplementary Figures S4(a) and (b) and Supplementary Table S1).

3.2. Fixed-bed column adsorption

Unlike batch adsorption, in column studies, the adsorbent at the inlet end is continuously contacted with the contaminated water. The change in heavy metal concentration at each succeeding layer is small, and accordingly, the adsorbent in the column will act like a series of layers, in which each layer is in contact with a fresh solution of constant heavy metal concentration. This continuous adsorption of the solute in the bed will result in maximum loading of the adsorbent (high x/M on the adsorption isotherm) at constant heavy metal concentration. This condition does not occur in the batch study because, unlike column adsorption, batch processes have a continuously dropping solute concentration. The MTZ is the active surface of the adsorbent material where heavy metal adsorption occurs. As the volume of heavy metal solution passing through the column increases, the mass transfer zone moves downward through the bed. After some time, the effluent concentration starts to increase, and when the MTZ reaches the exit of the bed, the effluent concentration becomes equal to the influent concentration. Hence, breakthrough and exhaustion are defined as the phenomena when the ratios of effluent-to-influent concentrations are 10 and 90%, respectively.

The breakthrough curves for different column operations, such as initial concentration, flow rate, and bed height, were investigated. In all cases, the adsorption capacity (q_c) and the breakthrough point time (t_b) were determined, and the breakthrough curves were used to validate the models.

3.3. Effect of influent metal concentration

In the present study, the effect of influent concentration of Pb, Cd, and Zn was investigated using a synthetic solution containing 10, 50, and 100 mg/L of metal ions at optimised flow rate (2 mL/min) and bed height (2 cm). The breakthrough curves of Pb, Cd, and Zn are shown in Figure 1, and the values of the experimental breakthrough parameters are tabulated in Table 3.

The breakthrough curves demonstrated that the breakthrough time and exhaustion time were inversely related to the influent metal concentration. At higher initial concentrations, the breakthrough curves shifted to the left side, and early breakthrough points are observed. This behaviour may be explained by the fact that the available adsorbent sites become saturated more quickly at higher influent metal ion concentrations and that results in reduced breakthrough time (Naja & Volesky 2008). Furthermore, it was observed that the adsorption capacity and the height of MTZ increased with the increase in initial metal concentration, whereas the removal efficiency was substantially decreased. The reason is that when the fixed-

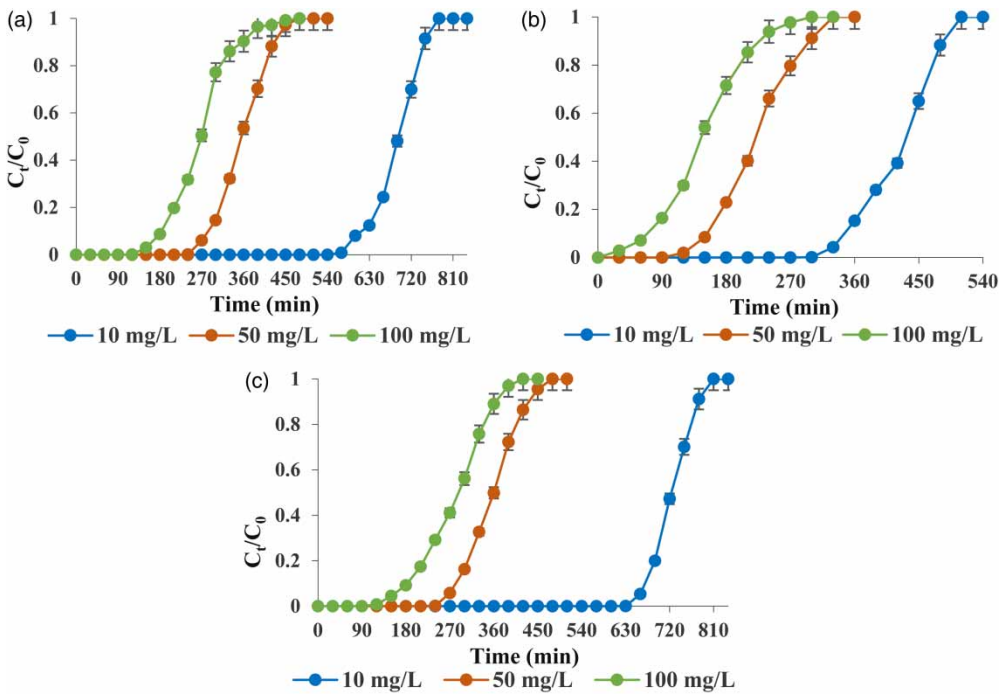

Figure 1 | Effect of the initial metal concentration on the breakthrough curves of (a) Pb, (b) Cd, and (c) Zn (flow rate, 2.0 mL/min; bed height, 2.0 cm; pH, 5 for Pb and 7 for Cd and Zn).

Table 3 | Parameters obtained from the breakthrough curves of the fixed-bed column

Metal	Influent metal concentration (mg/L)	Flow rate (mL/min)	Bed height (cm)	t_b (min)	t_e (min)	q_e (mg/g)	%R	MTZ (cm)
Pb	10	2	2	600	750	10.33	89	0.4
	50	2	2	270	420	23.34	72	0.71
	100	2	2	180	360	42.30	69	1.0
	50	1	2	540	750	24.06	86	0.56
	50	3	2	150	300	22.55	64	1.0
	50	2	4	450	660	24.68	82	1.27
	50	2	6	780	990	25.66	87	1.27
Cd	10	2	2	330	480	6.40	77	0.62
	50	2	2	150	300	15.05	64	1.0
	100	2	2	90	210	22.84	61	1.42
	50	1	2	330	510	16.70	78	0.70
	50	3	2	30	180	11.86	54	1.6
	50	2	4	360	540	19.38	78	1.33
	50	2	6	570	750	20.68	85	1.44
Zn	10	2	2	660	780	10.81	88	0.30
	50	2	2	270	390	23.03	76	0.61
	100	2	2	240	360	47.56	78	0.67
	50	1	2	570	750	25.79	84	0.48
	50	3	2	180	300	22.94	67	0.8
	50	2	4	510	660	25.19	86	0.91
	50	2	6	720	870	26.06	92	1.03

bed column reaches saturation, the amount of adsorbed metal ions is very low in comparison to the amount of metal ions passing through the column (Cruz-Olivares *et al.* 2013). The difference in metal removal efficiencies between 50 and 100 mg/L is less than the removal efficiencies between 50 and 10 mg/L. This could be explained by the fact that a higher inlet concentration provides a higher driving force for adsorption due to the increased concentration gradient between the surface of the sorbent and the solution. And the increase in the diffusion coefficient or mass transfer coefficient, due to this larger concentration gradient, will lead to faster transport, and hence increase the adsorption capacity (Samuel *et al.* 2013; Ravikumar *et al.* 2019).

It was found that with an increase in Pb(II) concentration from 10 to 100 mg/L, the corresponding adsorption capacity (q_e) increased from 10.33 to 42.30 mg/g. The percentage removal (%R) was calculated and found to be 89, 72, and 69% for the initial Pb(II) concentration of 10, 50, and 100 mg/L, respectively. As the influent concentration increased, the MTZ length increased from 0.1 to 1.0 cm for 10 and 100 mg/L, respectively (Table 3). The adsorption capacity increased from 6.40 to 22.84 mg/g when the initial concentration increased from 10 to 100 mg/L. The %R at 10, 50, and 100 mg/L Cd(II) concentrations were 77, 64, and 61%, respectively, and the MTZ, respectively, were 0.62, 1, and 1.42 cm. The adsorption capacity was increased from 10.81 to 23.03 mg/g and from 23.03 to 47.56 mg/g with an initial concentration of 10 to 50 mg/L and from 50 to 100 mg/L, respectively, for Zn(II). It was also noted that %R decreased from 88 to 78% with an increase in the Zn(II) concentration. The MTZ obtained were 0.30, 0.71, and 0.77 cm for initial concentrations of 10, 50, and 100 mL/min, respectively.

After analysing the effects of the initial concentration on Pb, Cd, and Zn and considering the concentration of real industrial wastewater, the optimal concentration was determined at 50 mg/L and it was chosen for the following experiments.

3.4. Effect of flow rate

The effect of flow rate on the adsorption of Pb, Cd, and Zn utilising P(St-DVB)/CuNi BNC was investigated by varying the flow rates (1, 2, and 3 mL/min) while the influent metal ion concentration was kept constant at 50 mg/L and the bed height was 2 cm.

The breakthrough curves clearly show that the breakthrough occurred significantly faster with an increase in flow (Figure 2). This could be due to the inadequate residence time of the heavy metals in the column and decreased diffusion of the heavy metals into the pore of the adsorbent at higher flow rates (Bulgariu & Bulgariu 2013; Han *et al.* 2009). Meanwhile, calculated values of the adsorption capacity and removal efficiency were found to decrease with an increase in flow

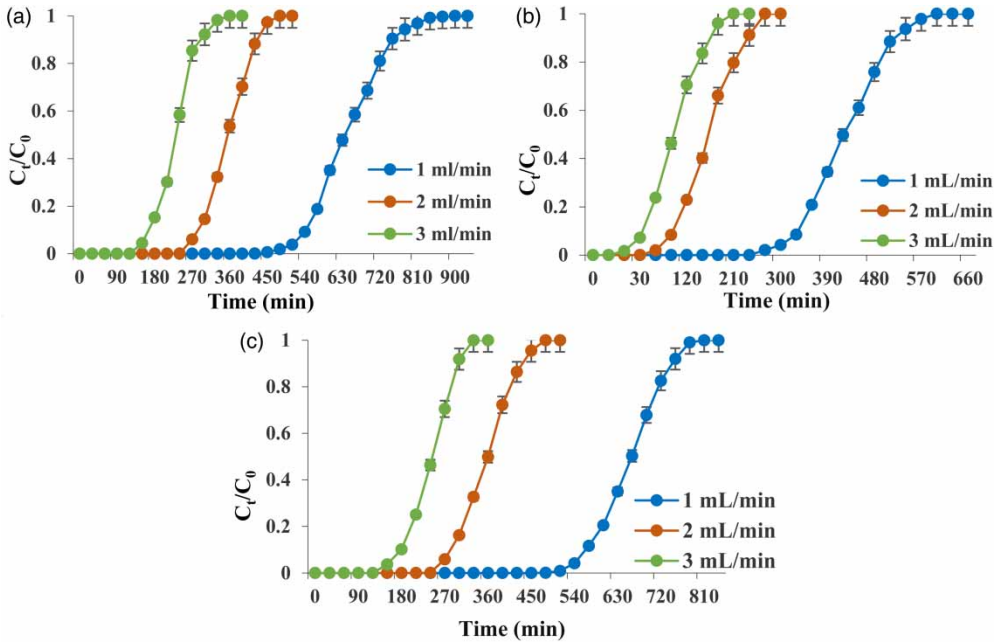

Figure 2 | Effect of flow rate on breakthrough curves of (a) Pb, (b) Cd, and (c) Zn (influent metal concentration, 50 mg/L; bed height, 2.0 cm; pH, 5 for Pb and 7 for Cd and Zn).

rate from 1 to 3 mL/min. The reduction in q_e values at higher flow rates can also be attributed to the insufficient contact time required for the heavy metals to interact with the adsorbent (Maiti *et al.* 2009; Mona *et al.* 2013). The mass transfer zone (MTZ) increased with increasing flow rate, and a similar observation was reported by Bulgariu & Bulgariu (2013).

The estimated lead removal efficiencies were 86, 72, and 64% for 1, 2, and 3 mL/min flow rates, respectively. It was also found that the adsorption capacity of the column decreases from 24.06 to 23.34 mg/g and 23.34 to 22.55 mg/g with an increased flow rate. Similar results were also obtained for cadmium and zinc. In the case of Cd, the adsorption capacities for flow rates of 1, 2, and 3 mL/min were 16.70, 15.05, and 11.86 mg/g, respectively, and the percentage removal obtained for the corresponding flow rates was 78, 64, and 54%, respectively. The Zn(II) adsorption capacity for tested flow rates of 1, 2, and 3 mL/min was 25.79, 23.03, and 22.94 mg/g, respectively, and the percentage removal obtained was 84, 76, and 67%, respectively.

Taking into account the results, the best performance was obtained at the lowest flow rate of 1.0 mL/min. However, at this flow rate, the run time and energy costs were very high, so the flow rate of 2.0 mL/min was applied in the next experiments.

3.5. Effect of bed height

The influence of bed height was investigated by raising it from 2 to 6 cm while maintaining a constant flow rate of 2 mL/min and inlet heavy metal concentration of 50 mg/L. The resulting lead, cadmium, and zinc breakthrough curves obtained at three different adsorbent masses can be observed in Figure 3.

An increase in t_b, q_e, and %R was observed with an increase in bed height. This could be attributed to the fact that there is an increase in absorbent doses in larger beds, which provide greater surface area and a higher number of adsorption sites (Baral *et al.* 2009; Sarkar & Das 2016). Jain *et al.* (2013) also reported a positive correlation between adsorption capacity and bed height (Jain *et al.* 2013). It was also observed that MTZ values increased with an increase in bed height, and this may be due to the increase in contact time for metal adsorption because of the higher adsorbent dosage (Singh *et al.* 2012).

In the present study, the lead breakthrough time and its adsorption capacity were increased from 23.34 to 25.66 mg/g and from 270 to 780 min, respectively, with increasing bed height from 2 to 6 (Figure 3). 72–87% of lead was removed by P(St-DVB)/CuNi BNC when the bed height of the adsorbent ranged from 2 to 6 cm. The calculated values of the adsorption capacities showed that it increased from 15.05 to 20.68 mg/g with an increase in bed height from 2 to 6 cm, respectively, for cadmium. The results also revealed that by increasing the bed height from 2 to 6 cm the percentage of Cd removal

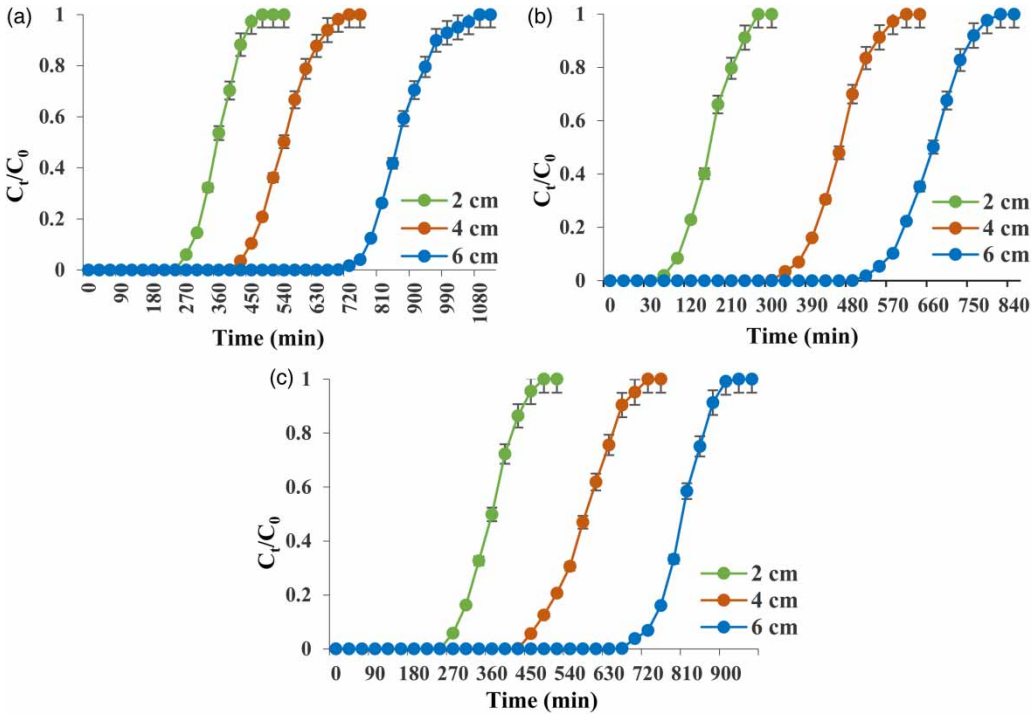

Figure 3 | Effect of bed height on breakthrough curves of (a) Pb, (b) Cd, and (c) Zn (flow rate, 2.0 mL/min; initial concentration of Zn (II), 50 mg/L; pH, 5 for Pb and 7 for Cd and Zn).

increased from 64 to 87% and the length of the MTZ increased from 1 to 1.44 cm. And in the case of zinc ions, the adsorption capacity was found to increase from 23.03 to 26.06 mg/g with an increasing bed depth of 2 to 6 cm, respectively, and the percentage removal was 76, 86 and 92% for bed heights 2, 4 and 6 cm, respectively.

According to the breakthrough parameters and the results of the fixed-bed column, zinc took the highest period to achieve the breakthrough concentration and cadmium took the least. This indicated that among the three metals, zinc adsorbed the most and cadmium the least onto P(St-DVB)/CuNi BNC.

Hence, to conclude, the lower influent concentration, lower flow rate, and higher bed height increased the adsorption of metal ions into the P(St-DVB)/CuNi BNC microspheres. Furthermore, these results were consistent with the findings established from our batch study (Hridya *et al.* 2021).

3.6. Modelling of breakthrough curves

Thomas, Yoon–Nelson, and Adams–Bohart models were applied to the breakthrough curves, and the values of characteristic parameters are presented in Tables 4–6, respectively.

3.6.1. Thomas model

The Thomas rate constant (k_{Th}) and the maximum adsorption capacity (q_0) were determined by fitting the experimental column data to the Thomas model. The values of k_{Th}, q_0, and the regression coefficient (R^2) at three different initial influent metal ion concentrations, flow rates, and bed heights are listed in Table 4. As observed in Table 4, the values of q_0 calculated from the Thomas model (Equation (1)) were comparable to the experimental q_e values. It was found that the values of q_0 increased with increasing influent metal ion concentration and bed depth, but decreased with increased flow rate. However, k_{Th} values significantly decreased with increasing influent metal ion concentration because the driving force for adsorption is the difference in concentration between the adsorbed metal ions on the adsorbent and its concentration in the solution, and the obtained results are consistent with the findings of other researchers (Sarin *et al.* 2006; Wu & Yu 2008). Furthermore, k_{Th} increased with increasing flow rates, while it reduced with increasing bed height. The rise in k_{Th} values with higher flow rates can be attributed to a decrease in mass transport resistance, while the drop in k_{Th} values with higher bed heights may be

Table 4 | Parameters of the Thomas model at different conditions

	Pb			Cd			Zn		
Parameters	k_{Th} (mL/min mg)	q_0 (mg/g)	R^2	k_{Th} (mL/min mg)	q_0 (mg/g)	R^2	k_{Th} (mL/min mg)	q_0 (mg/g)	R^2
Influent metal conc. (mg/L)									
10	3.50	10.79	0.971	3.05	6.90	0.979	3.58	11.41	0.982
50	0.66	23.38	0.989	0.66	16.22	0.996	0.65	23.52	0.996
100	0.26	42.75	0.996	0.29	23.04	0.999	0.27	47.71	0.978
Flow rate (mL/min)									
1	0.50	24.18	0.985	0.48	17.11	0.994	0.59	25.91	0.972
2	0.66	23.38	0.989	0.66	16.22	0.996	0.65	23.52	0.996
3	0.76	22.34	0.995	0.72	12.01	0.991	0.74	23.14	0.994
Bead height (cm)									
2	0.66	23.38	0.989	0.66	16.22	0.996	0.65	23.52	0.996
4	0.49	24.96	0.992	0.55	19.85	0.998	0.46	25.12	0.992
6	0.43	25.88	0.977	0.52	20.64	0.993	0.42	25.83	0.966

Table 5 | Parameters of the Yoon–Nelson model at different conditions

	Pb			Cd			Zn		
Parameters	k_{YN} (min^{-1})	τ (min)	R^2	k_{YN} (min^{-1})	τ (min)	R^2	k_{YN} (min^{-1})	τ (min)	R^2
Influent metal conc. (mg/L)									
10	0.031	618.56	0.974	0.031	417.53	0.979	0.036	721.82	0.982
50	0.032	303.07	0.989	0.033	205.76	0.996	0.031	326.31	0.996
100	0.033	218.32	0.996	0.034	122.87	0.999	0.027	307.0	0.978
Flow rate (mL/min)									
1	0.025	563.59	0.981	0.024	418.95	0.994	0.030	654.0	0.972
2	0.032	303.07	0.989	0.033	205.76	0.996	0.031	326.31	0.996
3	0.038	192.33	0.995	0.036	96.50	0.991	0.037	212.85	0.994
Bead height (cm)									
2	0.032	303.07	0.989	0.033	205.76	0.996	0.031	326.31	0.996
4	0.024	534.57	0.992	0.028	450.56	0.998	0.025	571.58	0.992
6	0.022	848.88	0.977	0.026	654.28	0.993	0.023	792.94	0.966

caused by an increase in mass transport resistance. The maximum Thomas adsorption capacity for heavy metals, Pb, Cd, and Zn, respectively, was achieved at 42.75, 23.04, and 47.71 mg/g.

The correlation coefficient R^2 values range from 0.971 to 0.996 for lead, 0.979 to 0.999 for cadmium, and 0.966 to 0.996 for zinc. This indicates that the Thomas model exhibited an excellent fit to the experimental data for all the parameters studied. The Thomas model predicts monolayer adsorption/desorption and the rate driving force follows second-order reversible reaction kinetics, which is also confirmed by our earlier batch sorption studies, where the experimental data fit very well with Langmuir isotherm. Therefore, we can conclude that the experiment follows monolayer adsorption and second-order reversible reaction kinetics, and external and internal diffusions were not the rate-limiting processes (Han *et al.* 2009; Chen *et al.* 2012).

3.6.2. Yoon–Nelson model

The Yoon–Nelson model was applied to investigate the breakthrough behaviour of Pb(II), Cd(VI), and Zn(II) adsorption on P(St-DVB)/CuNi BNC. The values of the Yoon-Nelson model rate constant k_{YN}, 50% breakthrough time τ, and the regression

Table 6 | Parameters of the Adams–Bohart model at different conditions

	Pb			Cd			Zn		
Parameters	$k_{AB} \times 10^{-3}$ (L/mg min)	N_0 (mg/L)	R^2	$k_{AB} \times 10^{-3}$ (L/mg min)	N_0 (mg/L)	R^2	$k_{AB} \times 10^{-3}$ (L/mg min)	N_0 (mg/L)	R^2
Influent metal conc. (mg/L)									
10	1.48	2,448.99	0.951	1.82	1,561.83	0.929	1.73	2,493.21	0.963
50	0.299	6,872.58	0.901	0.403	4,455.01	0.878	0.336	6,369.43	0.895
100	0.118	11,837.1	0.832	0.165	6,835.08	0.916	0.126	12,789.4	0.935
Flow rate (mL/min)									
1	0.269	6,147.82	0.78	0.243	4,147.48	0.888	0.312	5,898.80	0.849
2	0.299	6,872.58	0.901	0.403	4,455.01	0.878	0.336	6,369.43	0.895
3	0.332	7,150.24	0.865	0.442	3,699.8	0.805	0.422	7,005.36	0.949
Bead height (cm)									
2	0.299	6,872.58	0.901	0.403	4,455.01	0.878	0.336	6,369.43	0.895
4	0.247	6,146.78	0.836	0.276	4,308.68	0.897	0.225	5,318.43	0.926
6	0.214	5,419.16	0.781	0.277	3,970.51	0.894	0.321	4,668.57	0.925

coefficient (R^2) obtained for all breakthrough curves are given in Table 5. The k_{YN} was higher at higher influent metal ion concentrations. This is because the competition between the adsorbate species for the adsorption sites increases when the metal ion concentration increases, which ultimately results in a higher rate of retention. Moreover, the values of k_{YN} were found to increase with an increase in flow rates, whereas a reverse trend is observed for bed heights. However, the values of τ were found to decrease significantly with both increasing initial influent concentration and flow rate, while the τ values increased with an increase in bed height. This is because the saturation of the column was attained quickly when the initial influent concentration and flow rate increased, but considerably slower saturation of the column occurs at higher bed heights. Furthermore, the correlation coefficient values were found to be between 0.974 and 0.996 for lead, 0.979 and 0.999 for cadmium, and 0.966 and 0.996 for zinc, which shows the Yoon–Nelson model fitted well to the experimental data along with the Thomas model.

3.6.3. Adams–Bohart model

The values of kinetic constant, k_{AB} and saturation concentration, N_0 were calculated from the linear plots with respect to influent heavy metal concentration, flow rate, and bed height using the Adams–Bohart model given in Table 6 along with their correlation coefficients (R^2). The value of kAB decreased with both increasing influent concentration and depth of the column bed, while it increased with increasing flow rate. However, at the same time, the value of N_0 increased with increasing influent metal concentration and flow rate; nevertheless, it reduced with increasing bed height. The value of R^2 fluctuates from 0.781 to 0.951 for lead, 0.805 to 0.929 for cadmium, and 0.849 to 0.963 for zinc. The R^2 values show that the experiment data are fairly well described by the model but it is not the most suitable model to describe the experimental breakthrough curve.

In a comparison of predicted models, it is observed that the R^2 values of the Thomas and Yoon–Nelson models are higher than the Adams–Bohart model. Therefore, it can be concluded that both Thomas and Yoon–Nelson models can be used to predict the removal of metal ions by a fixed-bed column packed with P(St-DVB)/CuNi BNC microbeads.

3.7. Desorption experiments

The desorption of heavy metals from the P(St-DVB)/CuNi BNC microsphere was carried out with 0.5 M concentrations of NaOH solution because this concentration of NaOH showed a good desorption efficiency of heavy metal ions in batch desorption experiments. Desorption studies were conducted for up to four successive adsorption–desorption cycles. From the adsorption–desorption data, it was indicated that the removal efficiency (%) decreased with each adsorption–desorption cycle in progress for all investigated metals. Total regeneration was not achieved due to incomplete desorption of metal ions from the adsorbent (Table 7). The removal efficiency decreased from 70 to 56%, 63 to 50%, and 73 to 59%, respectively,

Table 7 | Desorption studies of the studied ions from P(St-DVB)/CuNi BNC microspheres

	Removal efficiency (%)			
Metals	**Cycle 1**	**Cycle 2**	**Cycle 3**	**Cycle 4**
Pb	70	67	63	56
Cd	63	61	57	50
Zn	73	70	66	59

for Pb, Cd, and Zn from cycle 1 to cycle 4. This preliminary study suggests that the P(St-DVB)/CuNi BNC microsphere is a potential adsorbent for the removal of heavy metal ions in a fixed-bed column with repeated usage.

4. CONCLUSION

The removal of lead, cadmium, and zinc using P(St-DVB)/CuNi BNC microspheres in a fixed-bed column was investigated by varying the process parameters such as initial metal concentration, flow rate, and bed height, and the breakthrough curves were plotted. Experimental results revealed that the increase in flow rate and influent metal concentrations significantly affected the column performance by decreasing the breakthrough, exhaustion time, and total removal efficiency of heavy metals. On the contrary, the increase in bed height tended to increase the breakthrough and exhaustion time of the column, and hence the higher percentage of heavy metal removal. The adsorption capacity was increased with increasing initial metal concentration, increasing bed height, and decreasing flow rate. The maximum percentages of heavy metals achieved by nanocomposite were 87, 85, and 92% for lead, cadmium, and zinc, respectively. The obtained breakthrough and the column kinetic parameters were successfully predicted with mathematical models such as the Thomas, Yoon–Nelson, and Adams–Bohart models, and both Thomas and Yoon–Nelson models were shown to be in good agreement with the experimental results for all operating conditions studied. The successful desorption of heavy metals from the P(St-DVB)/CuNi BNC microspheres was performed using NaOH solution and showed good reusability of the adsorbent in the bed column during four adsorption–desorption cycles. The removal efficiency decreased from 70 to 56%, 63 to 50%, and 73 to 59%, respectively, for Pb, Cd, and Zn from cycle 1 to cycle 4. The results show that P(St-DVB)/CuNi BNC microspheres are an effective and low-cost adsorbent, and it can be used in real-time large-scale industrial water treatment processes for the removal of heavy metals. Moreover, there is a wide scope of improvement in terms of nanomaterial functionalities, uptake capacities, and robustness for adsorption-based purification techniques. Therefore, further research and significant efforts are required to scale up the processes for taking laboratory-based techniques to pilot-scale methods with better efficiencies.

ACKNOWLEDGEMENTS

The current work was financially supported by the Council of Scientific & Industrial Research (CSIR), India [Sanction no: 09/1195(0001)/2018-EMR-I].

AUTHORS' CONTRIBUTIONS

T. K. Hridya conceptualised the whole article, devised the methodology, validated the article, and wrote the original draft. Rosmin Antu investigated the article; Harikumar PS supervised the process, wrote the review and edited the article.

DATA AVAILABILITY STATEMENT

All relevant data are included in the paper or its Supplementary Information.

CONFLICT OF INTEREST

The authors declare there is no conflict.

REFERENCES

Agrawal, P. & Bajpai, A. K. 2011 Dynamic column adsorption studies of toxic Cr (VI) ions onto iron oxide loaded gelatin nanoparticles. *Journal of Dispersion Science and Technology* **32** (9), 1353–1362.

Ahmad, A. A. & Hameed, B. H. 2010 Fixed-bed adsorption of reactive azo dye onto granular activated carbon prepared from waste. *ournal of Hazardous Materials* **175** (1–3), 298–303.

Aksu, Z. & Gönen, F. 2004 Biosorption of phenol by immobilized activated sludge in a continuous packed bed: prediction of breakthrough curves. *Process Biochemistry* **39** (5), 599–613.

Aksu, Z., Çağatay, Ş. Ş. & Gönen, F. 2007 Continuous fixed bed biosorption of reactive dyes by dried *Rhizopus arrhizus*: determination of column capacity. *Journal of Hazardous Materials* **143** (1–2), 362–371.

Barakat, M. A. 2011 New trends in removing heavy metals from industrial wastewater. *Arabian Journal of Chemistry* **4** (4), 361–377.

Baral, S. S., Das, N., Ramulu, T. S., Sahoo, S. K., Das, S. N. & Chaudhury, G. R. 2009 Removal of Cr (VI) by thermally activated weed *Salvinia cucullata* in a fixed-bed column. *Journal of Hazardous Materials* **161** (2–3), 1427–1435.

Bohart, G. S. & Adams, E. Q. 1920 Some aspects of the behavior of charcoal with respect to chlorine. *Journal of the American Chemical Society* **42** (3), 523–544.

Bulgariu, D. & Bulgariu, L. 2013 Sorption of Pb (II) onto a mixture of algae waste biomass and anion exchanger resin in a packed-bed column. *Bioresource Technology* **129**, 374–380.

Chen, S., Yue, Q., Gao, B., Li, Q., Xu, X. & Fu, K. 2012 Adsorption of hexavalent chromium from aqueous solution by modified corn stalk: a fixed-bed column study. *Bioresource Technology* **113**, 114–120.

Chen, L., Ji, T., Mu, L., Shi, Y., Brisbin, L., Guo, Z., Khan, M. A., Young, D. P. & Zhu, J. 2016 Facile synthesis of mesoporous carbon nanocomposites from natural biomass for efficient dye adsorption and selective heavy metal removal. *RSC Advances* **6** (3), 2259–2269.

Cruz-Olivares, J., Pérez-Alonso, C., Barrera-Díaz, C., Ureña-Nuñez, F., Chaparro-Mercado, M. C. & Bilyeu, B. 2013 Modeling of lead (II) biosorption by residue of allspice in a fixed-bed column. *Chemical Engineering Journal* **228**, 21–27.

De Kwaadsteniet, M., Dobrowsky, P. H., Van Deventer, A., Khan, W. & Cloete, T. E. 2013 Domestic rainwater harvesting: microbial and chemical water quality and point-of-use treatment systems. *Water, Air, & Soil Pollution* **224** (7), 1–19.

Han, R., Zou, L., Zhao, X., Xu, Y., Xu, F., Li, Y. & Wang, Y. 2009 Characterization and properties of iron oxide-coated zeolite as adsorbent for removal of copper (II) from solution in fixed bed column. *Chemical Engineering Journal* **149** (1–3), 123–131.

Harikumar, P. S. & Hridya, T. K. 2021 Application of CuNi bimetallic nanoparticle as an adsorbent for the removal of heavy metals from aqueous solution. *International Journal of Environmental Analytical Chemistry* **101** (6), 869–883.

Hridya, T., Varghese, E. & Harikumar, P. S. 2021 Removal of heavy metals from aqueous solution using porous (Styrene-divinylbenzene)/CuNi bimetallic nanocomposite microspheres. *Environmental Nanotechnology, Monitoring & Management* **16**, 100606.

Jain, M., Garg, V. K. & Kadirvelu, K. 2013 Cadmium (II) sorption and desorption in a fixed bed column using sunflower waste carbon calcium–alginate beads. *Bioresource Technology* **129**, 242–248.

Li, W., Yue, Q., Tu, P., Ma, Z., Gao, B., Li, J. & Xu, X. 2011 Adsorption characteristics of dyes in columns of activated carbon prepared from paper mill sewage sludge. *Chemical Engineering Journal* **178**, 197–203.

Luo, X., Deng, Z., Lin, X. & Zhang, C. 2011 Fixed-bed column study for Cu^{2+} removal from solution using expanding rice husk. *Journal of Hazardous Materials* **187** (1–3), 182–189.

Maiti, S. K., Bera, D., Chattopadhyay, P. & Ray, L. 2009 Determination of kinetic parameters in the biosorption of Cr (VI) on immobilized *Bacillus cereus* M 1 16 in a continuous packed bed column reactor. *Applied Biochemistry and Biotechnology* **159**, 488–504.

McNabb, D. E. 2019 The population growth barrier. In: *Global Pathways to Water Sustainability* (D. E. McNabb, ed.) Palgrave Macmillan, Cham, pp. 67–81.

Mona, S., Kaushik, A. & Kaushik, C. P. 2013 Prolonged hydrogen production by Nostoc in photobioreactor and multi-stage use of the biological waste for column biosorption of some dyes and metals. *Biomass and Bioenergy* **54**, 27–35.

Naja, G. & Volesky, B. 2008 Optimization of a biosorption column performance. *Environmental Science & Technology* **42** (15), 5622–5629.

Nriagu, J. O. & Pacyna, J. M. 1988 Quantitative assessment of worldwide contamination of air, water and soils by trace metals. *Nature* **333** (6169), 134–139.

Nuić, I., Trgo, M., Perić, J. & Medvidović, N. V. 2013 Analysis of breakthrough curves of Pb and Zn sorption from binary solutions on natural clinoptilolite. *Microporous and Mesoporous Materials* **167**, 55–61.

Olvera, R. C., Silva, S. L., Robles-Belmont, E. & Lau, E. Z. 2017 Review of the nanotechnology value chain for water treatment applications in Mexico. *Resource-Efficient Technologies* **3** (1), 1–11.

Omer, A., Elagib, N. A., Zhuguo, M., Saleem, F. & Mohammed, A. 2020 Water scarcity in the Yellow River Basin under future climate change and human activities. *Science of the Total Environment* **749**, 141446.

Pehlivan, E., Yanık, B. H., Ahmetli, G. & Pehlivan, M. 2008 Equilibrium isotherm studies for the uptake of cadmium and lead ions onto sugar beet pulp. *Bioresource Technology* **99** (9), 3520–3527.

Ravikumar, K. V. G., Singh, A. S., Sikarwar, D., Gopal, G., Das, B., Mrudula, P., Natarajan, C. & Mukherjee, A. 2019 Enhanced tetracycline removal by in-situ NiFe nanoparticles coated sand in column reactor. *Journal of Environmental Management* **236**, 93–99.

Rijsberman, F. R. 2006 Water scarcity: fact or fiction? *Agricultural Water Management* **80** (1–3), 5–22.

Samuel, J., Pulimi, M., Paul, M. L., Maurya, A., Chandrasekaran, N. & Mukherjee, A. 2013 Batch and continuous flow studies of adsorptive removal of Cr (VI) by adapted bacterial consortia immobilized in alginate beads. *Bioresource Technology* **128**, 423–430.

Sandia, D. 2003 *Water Purification Roadmap – A Report of the Executive Committee*. US Department of the Interior, Bureau of Reclamation and Sandia National Laboratories. Report.

Sarin, V., Singh, T. S. & Pant, K. K. 2006 Thermodynamic and breakthrough column studies for the selective sorption of chromium from industrial effluent on activated eucalyptus bark. *Bioresource Technology* **97** (16), 1986–1993.

Sarkar, S. & Das, S. K. 2016 Removal of Cr (VI) and Cu (II) ions from aqueous solution by rice husk ash – column studies. *Desalination and Water Treatment* **57** (43), 20340–20349.

Schwarzenbach, R. P., Egli, T., Hofstetter, T. B., Von Gunten, U. & Wehrli, B. 2010 Global water pollution and human health. *Annual Review of Environment and Resources* **35** (1), 109–136.

Sharma, G., Naushad, M., Kumar, A., Devi, S. & Khan, M. R. 2015 Lanthanum/Cadmium/Polyaniline bimetallic nanocomposite for the photodegradation of organic pollutant. *Iranian Polymer Journal* **24** (12), 1003–1013.

Sharma, G., Kumar, A., Sharma, S., Naushad, M., Dwivedi, R. P., ALOthman, Z. A. & Mola, G. T. 2019 Novel development of nanoparticles to bimetallic nanoparticles and their composites: a review. *Journal of King Saud University-Science* **31** (2), 257–269.

Singh, A., Kumar, D. & Gaur, J. Á. 2012 Continuous metal removal from solution and industrial effluents using Spirogyra biomass-packed column reactor. *Water Research* **46** (3), 779–788.

Taner, M., Sayar, N., Yulug, I. G. & Suzer, S. 2011 Synthesis, characterization and antibacterial investigation of silver–copper nanoalloys. *Journal of Materials Chemistry* **21** (35), 13150–13154.

Tchounwou, P. B., Yedjou, C. G., Patlolla, A. K. & Sutton, D. J. 2012 Heavy metal toxicity and the environment. *Molecular, Clinical and Environmental Toxicology* **101**, 133–164.

Thomas, H. C. 1944 Heterogeneous ion exchange in a flowing system. *Journal of the American Chemical Society* **66** (10), 1664–1666.

Wadhawan, S., Jain, A., Nayyar, J. & Mehta, S. K. 2020 Role of nanomaterials as adsorbents in heavy metal ion removal ions from waste water: a review. *Journal of Water Process Engineering* **33**, 101038.

Wu, J. & Yu, H. Q. 2008 Biosorption of 2, 4-dichlorophenol from aqueous solutions by immobilized *Phanerochaete chrysosporium* biomass in a fixed-bed column. *Chemical Engineering Journal* **138** (1–3), 128–135.

Yagub, M. T., Sen, T. K., Afroze, S. & Ang, H. M. 2015 Fixed-bed dynamic column adsorption study of methylene blue (MB) onto pine cone. *Desalination and Water Treatment* **55** (4), 1026–1039.

Yoon, Y. H. & Nelson, J. H. 1984 Application of gas adsorption kinetics I. A theoretical model for respirator cartridge service life. *American Industrial Hygiene Association Journal* **45** (8), 509–516.

First received 7 January 2023; accepted in revised form 21 March 2023. Available online 13 April 2023